Journal of Biomechanics 48 (2015) 4287–4296

Contents lists available at ScienceDirect

Journal of Biomechanics

journal homepage: www.elsevier.com/locate/jbiomech
www.JBiomech.com

Material modeling of cardiac valve tissue: Experiments, constitutive analysis and numerical investigation

Stefanie Heyden [a,*], Andreas Nagler [b], Cristóbal Bertoglio [b,d], Jonas Biehler [b], Michael W. Gee [c], Wolfgang A. Wall [b], Michael Ortiz [a]

[a] Computational Mechanics Group, California Institute of Technology, USA
[b] Institute for Computational Mechanics, Technische Universität München, Germany
[c] Mechanics & High Performance Computing Group, Technische Universität München, Germany
[d] Center for Mathematical Modeling, Universidad de Chile, Chile

ARTICLE INFO

Article history:
Accepted 26 October 2015

Keywords:
Cardiac valves
Tensile tests
Constitutive modeling
Parameter estimation
Finite element analysis

ABSTRACT

A key element of the cardiac cycle of the human heart is the opening and closing of the four valves. However, the material properties of the leaflet tissues, which fundamentally contribute to determine the mechanical response of the valves, are still an open field of research. The main contribution of the present study is to provide a complete experimental data set for porcine heart valve samples spanning all valve and leaflet types under tensile loading. The tests show a fair degree of reproducibility and are clearly indicative of a number of fundamental tissue properties, including a progressively stiffening response with increasing elongation. We then propose a simple anisotropic constitutive model, which is fitted to the experimental data set, showing a reasonable interspecimen variability. Furthermore, we present a dynamic finite element analysis of the aortic valve to show the direct usability of the obtained material parameters in computational simulations.

1. Introduction

The mechanical modeling of cardiac valve tissues has a long-standing history during which increasingly refined experimental setups and constitutive models have been developed. Early on, experimental testing revealed the highly nonlinear and anisotropic nature of cardiac valve tissues. In Clark (1973), aortic as well as mitral valve leaflets were examined under uniaxial tensile loading, showing a more compliant tissue behavior in the radial direction (perpendicular to the annulus). In Thubrikar et al. (1980), this finding was later confirmed using in vivo tests (via radiopaque markers) and in vitro measurements (by recourse to tensile testing after euthanization). In order to investigate the effects of chemical treatment for bioprosthetic heart valve replacements, biaxial mechanical tests on native and glutaraldehyde-treated porcine aortic valve cusps were performed (Billiar and Sacks, 2000b). Thereby, chemical treatment was shown to significantly lower tissue extensibility. Taking the layered structure of aortic valve tissue into account, strip biaxial tests on the separated ventricularis- and fibrosa layers were performed in Stella and Sacks (2007a), showing that both layers are characterized by a different anisotropic and nonlinear response, whereby the fibrosa layer dominates the mechanical response of the leaflet tissue. With regard to the time dependence in material behavior, the aortic valve's stress–strain response was found to be independent of strain rate (Stella and Sacks, 2007b), thereby confirming earlier studies, in which it was shown that after performing a sufficient number of preconditioning cycles, cardiac valve tissues do not exhibit viscoelastic effects on time scales comparable to the cardiac cycle (Fung, 1993). As a key characteristic typical to biological tissues, heart valve tissues were furthermore shown to not release their aqueous components under compressive loading and are therefore classified as incompressible (Hvidberg, 1960).

Ensuing from experimental investigations, a number of constitutive models based on general considerations of finite elasticity and anisotropy have been proposed in the literature. Thereby, prominant candidates consider contributions from an isotropic elastic matrix in combination with anisotropic exponential fiber terms (Billiar and Sacks, 2000a; Chen et al., 2004; Driessen et al., 2005; May-Newman and Yin, 1998; Prot et al., 2007, 2009; Soares et al., 2014) (some models furthermore consider inhomogeneities based on random fiber angles Billiar and Sacks, 2000a). In a recent investigation, the material parameters of such models were fitted from in vivo displacement measurements and finite element inverse analysis for mitral valve tissue (Rausch et al., 2013; Rausch and Kuhl, 2013). However, most previous studies are limited to

* Corresponding author.
E-mail address: heyden@caltech.edu (Stefanie Heyden).

http://dx.doi.org/10.1016/j.jbiomech.2015.10.043
0021-9290/

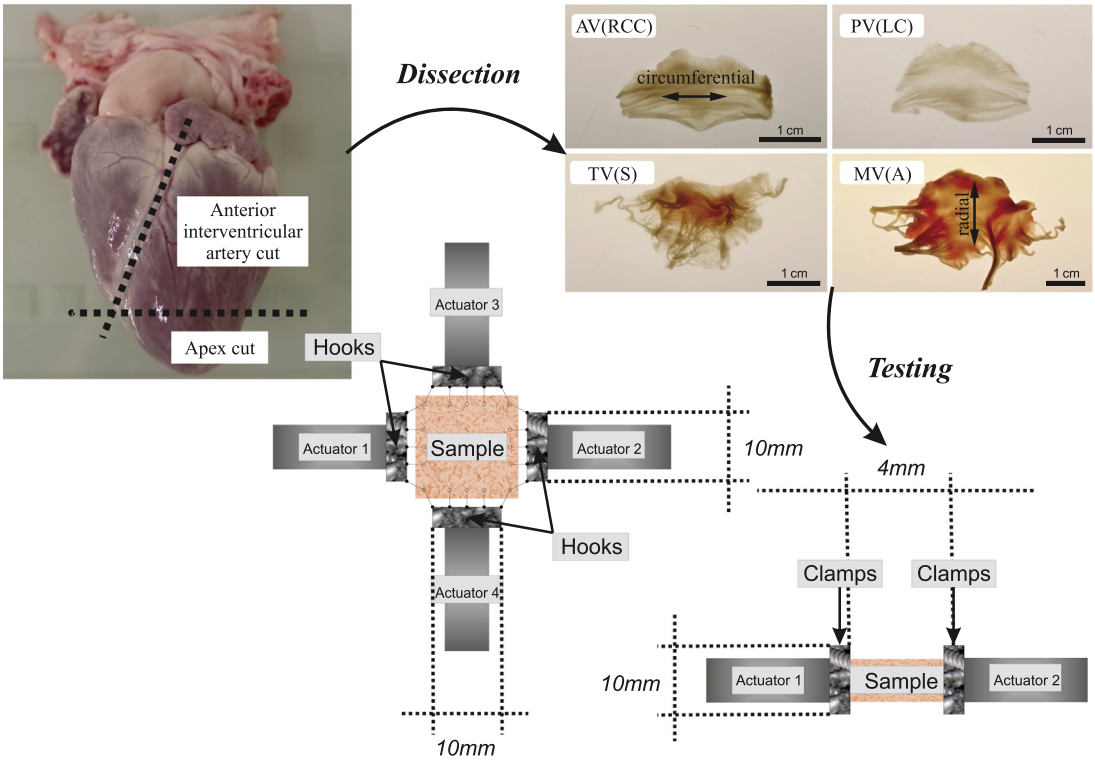

Fig. 1. Dissection of the porcine heart showing main cuts and sample leaflet types of the mitral (MV), tricuspid (TV), aortic (AV), and pulmonary valve (PV), depicted with the corresponding anatomical alignment (radial/circumferential). Harvested samples are used in the illustrated experimental setups (for purposes of detail representation, illustrations are not proportional and length measurements are added).

one particular valve type (see, e.g., Billiar and Sacks (2000b), Christie and Barratt-Boyes (1995), Lo and Vesely (1995), Stella and Sacks (2007a), Stella and Sacks (2007b)), and few studies to two valve types (see, e.g., Clark (1973), Soares et al. (2014)).

To the best of the authors knowledge, there are no works reported in the literature testing all different valve and leaflet types for several individuals under identical experimental conditions. Hence, the present contribution intends to broaden the understanding of the mechanical behavior of cardiac valve tissues by simultaneously:

(i) Performing tensile tests on porcine heart valve leaflets spanning all different valve and leaflet types under identical experimental conditions (Section 2.1) as our key contribution.
(ii) Proposing a simple and micromechanically sound constitutive model (including fiber angles) (Section 2.2).
(iii) Estimating the material constants of the proposed model for all tensile tests (Section 3.1).
(iv) Performing three-dimensional, dynamic finite element simulations of an aortic valve in order to validate that the obtained material constants lead to a physiological valve behavior (Section 3.2).

2. Materials and methods

2.1. Tissue samples and tensile experiments

A total of 87 leaflet samples was tested, spanning all four cardiac valves: the mitral valve (MV) comprising anterior (A) and posterior (P) leaflets; the aortic valve (AV) composed of the left and right coronary (LCC, RCC) and posterior (PC) cusps; the tricuspid valve (TV) consisting of the anterior (A), septal (S), and posterior (P) leaflets; and the pulmonary valve (PV) comprising the anterior (AC), the left (LC), and the right (RC) cusps.

In all cases, dissection of the porcine hearts occurred within a time frame of 3–7 h post mortem, during which the hearts were stored in water at a temperature of 4 °C. During the dissection process, three main cuts allowed for the opening of ventricles and atria, while leaving all valve leaflets intact. The first two cuts were placed along the anterior and posterior interventricular artery, and a final cut was placed right above the apex of the heart (see Fig. 1). Between dissection and testing, the heart leaflets were stored in culture dishes under the same storage conditions as the porcine hearts, with water exchanged every 24 h (within the given time frame during which samples are tested, which lies between 0 and 3 days, prior investigations on porcine aorta tissue performed in our group did not show differences in mechanical behavior between samples stored in physiological solution and samples stored in water). A summary of the different valve leaflets tested is given in Table 1. The larger sample sizes of mitral and tricuspid valve leaflets allowed for testing in the biaxial experimental setup, whereas the aortic and pulmonary valve leaflets were tested uniaxially in the circumferential direction parallel to the annulus, see Fig. 1.

Table 1
Number of harvested samples and ranges of estimated parameter values.

Valve	Harvested samples	Protocol	C (MPa)	G (MPa)	a (−)
AV	18	Uniaxial	0.1–0.95	10–212	2.5–3.6
PV	19	Uniaxial	0.2–0.59	8–157	2.5–3.6
MV	12	Uniaxial	0.1–0.13	5–45	2.5–3.6
MV	8	Biaxial	0.03–0.09	23–102	3.2–4.1
TV	21	Uniaxial	0.1–0.19	7–114	2.8–3.9
TV	14	Biaxial	0.04–0.09	7–114	2.8–4.0

For the experimental testing procedure, rectangular samples were cut from all leaflets. Subsequently, sample thicknesses were measured using a pressure sensitive gauge (Mitutoyo PK – 1012E). Measured mean thicknesses ($\pm$ standard deviation) for each leaflet type were obtained as: 0.63 ± 0.23 mm (TV-S), 0.69 ± 0.45 mm (TV-A), 0.55 ± 0.28 mm (TV-P), 0.66 ± 0.14 mm (MV-A), 0.87 ± 0.19 mm (MV-P), 0.48 ± 0.11 mm (AV-RCC), 0.51 ± 0.11 mm (AV-LCC), 0.52 ± 0.13 mm (AV-PC), 0.33 ± 0.09 mm (PV-RC), 0.32 ± 0.04 mm (PV-AC), and 0.31 ± 0.11 mm (PV-LC). In the uniaxial cases, samples were fixed using plastic clamps (which were positioned 4 mm apart from each other, see Fig. 1) with a torque wrench that applied a constant force of 0.7 N perpendicular to the tensile plane.

By way of example, an outline of the testing procedure for the uniaxial test case is described below. The samples were first preconditioned by holding them fixed at one end and uniaxially loading them at the other end by moving the actuator following a displacement-controlled procedure up to a maximum displacement corresponding to an applied force of 2 N, see example in Fig. 2. Afterwards, the

clamped sample was re-centered with respect to the measurement axis. Then, the data used for the material parameter fittings was generated by using a displacement controlled loading in the form of sine cycling, whereby both ends were moved. During the test procedure, samples were sprayed with water in order to keep them moisturized. For the biaxial testing procedure, hooks were used with a total of five hooks per side. The testing procedure then followed the same outline as in the uniaxial case, suitably modified to involve all four actuators. From the experimentally measured force–displacement curves for both uniaxial as well as biaxial test cases, first Piola–Kirchhoff (1PK) stresses are calculated from the measured axial forces using the mean thickness for each leaflet type as listed above.

2.2. Constitutive material model

Let us define $\mathbf{C}=\mathbf{F}^{\top}\mathbf{F}$ as the right Cauchy–Green deformation tensor, with $\mathbf{F}$ denoting the deformation gradient. In the following, we model cardiac valve tissue as an isotropic, incompressible matrix with embedded anisotropic collagenous fibers, as represented by the strain-energy density

$$W_{\text{valve}}(\mathbf{C})=W_{\text{matrix}}(\mathbf{C})+W_{\text{fiber}}(\mathbf{C}) \tag{1}$$

$$W_{\text{valve}}(\mathbf{C})=W_{\text{matrix}}(I_1,J)+\sum_{i=1}^{N}W_{\text{fiber}}(I_{4,i}), \tag{2}$$

whereby $I_1=\text{Tr}\,(\mathbf{C})$, $J^2=\det(\mathbf{C})$, $I_{4,i}=\mathbf{f}_i\ddot{A}\dot{n}(\text{Cf}_i)$, and $\mathbf{f}_i$ is the ith fiber direction. For the matrix contribution, we furthermore have

$$W_{\text{matrix}}(I_1,J)=C(I_1-3)+p(J-1), \tag{3}$$

with material constant $C\in\mathbb{R}^{+}$ and p as the Lagrangian multiplier arising from the incompressibility constraint $J\equiv 1$. For the strain-energy density term modeling fiber contributions, we then propose

$$W_{\text{fiber}}(I_{4,i})=G_i\left(|\sqrt{I_{4,i}}-1|_{+}\right)^{a_i},\quad i=1,\ldots,N \tag{4}$$

where G_i and a_i are the stiffness and exponent constants of the i th fiber family, respectively, and $|x|_{+}$ denotes the positive part of x.

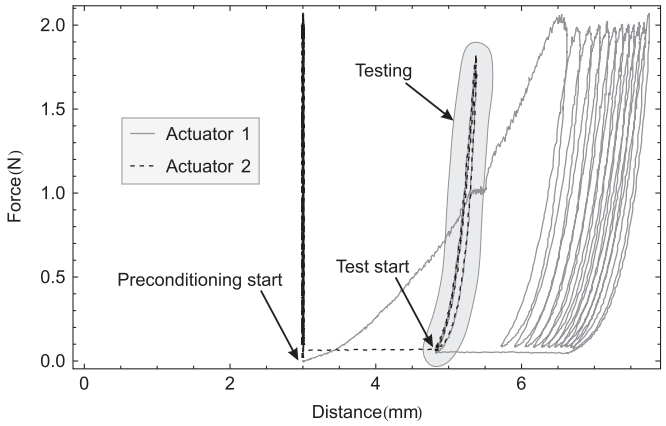

Fig. 2. Uniaxial preconditioning on a tricuspid valve leaflet using plastic clamps.

We recall that the first Piola–Kirchhoff stress tensor can be written as (Marsden and Hughes, 1983)

$$\mathbf{P}=2\frac{\partial W_{\text{matrix}}}{\partial I_1}\mathbf{F}-p\,\mathbf{F}^{-T}+\sum_{i=1}^{N}2\frac{\partial W_{\text{fiber}}}{\partial I_{4,i}}\mathbf{F}\,\mathbf{f}_i\otimes\mathbf{f}_i, \tag{5}$$

with

$$\frac{\partial W_{\text{matrix}}}{\partial I_1}=C\quad\text{and}\quad\frac{\partial W_{\text{fiber}}}{\partial I_{4,i}}=\frac{a_iG_i}{2\sqrt{I_{4,i}}}\left|\sqrt{I_{4,i}}-1\right|_{+}^{a_i-1}. \tag{6}$$

In order to find analytical expressions for the different stress components, we assume a deformation state described by pure normal strains, i.e., $\mathbf{F}=\text{diag}[\lambda_1\ \lambda_2\ \lambda_3]$. Moreover, the fibers are of the form $\mathbf{f}_i=[\cos\varphi_i,\sin\varphi_i,0]^{\top}$, whereby φ_i denotes the angle with respect to the uniaxial testing direction $[1,0,0]^{\top}$.

Hence, the components of $\mathbf{P}_{ii}$ can be written as

$$\mathbf{P}_{11}(\lambda_1,\lambda_2)=2\frac{\partial W_{\text{matrix}}}{\partial I_1}\lambda_1-p\frac{1}{\lambda_1}+\sum_{i=1}^{N}\frac{\partial W_{\text{fiber}}}{\partial I_{4,i}}\lambda_1\cos^2\varphi_i, \tag{7}$$

$$\mathbf{P}_{22}(\lambda_1,\lambda_2)=2\frac{\partial W_{\text{matrix}}}{\partial I_1}\lambda_2-p\frac{1}{\lambda_2}+2\sum_{i=1}^{N}\frac{\partial W_{\text{fiber}}}{\partial I_{4,i}}\lambda_2\sin^2\varphi_i, \tag{8}$$

$$\mathbf{P}_{33}(\lambda_3)=2\frac{\partial W_{\text{matrix}}}{\partial I_1}\lambda_3-p\frac{1}{\lambda_3}. \tag{9}$$

Under the assumption of planar tensile testing, we make use of the plane stress assumption $\mathbf{P}_{33}=0$ and additionally use the incompressibility condition $J=\det(\mathbf{F})=\lambda_1\lambda_2\lambda_3=1$, which enables us to derive a value for the Lagrange multiplier p as

$$p=2\lambda_3^2\frac{\partial W_{\text{matrix}}}{\partial I_1}=2\frac{1}{\lambda_1^2\lambda_2^2}\frac{\partial W_{\text{matrix}}}{\partial I_1}. \tag{10}$$

For the uniaxial test case in which only λ_1 and $\mathbf{P}_{11}$ are measured, we furthermore assume that $\mathbf{P}_{22}=0$. This gives an implicit relation between λ_1 and λ_2 following from Eq. (8) and hence leads to $\mathbf{P}_{11}=\mathbf{P}_{11}(\lambda_1,\lambda_2(\lambda_1))$. It bears mentioning that in uniaxial tests, because of the assumption of incompressibility, extension in one direction implies compression in the direction perpendicular to the loading axis. Fibers oriented around this axis are under compression and hence do not contribute to the material response. Therefore, only the parameters of one fiber family can be identified. For the biaxial test cases however, the second set of fibers oriented perpendicular to the first fiber family has to be taken into account. The derivation of expressions for the first Piola–Kirchhoff stress components then follows as outlined above.

2.3. Parameter fitting

We propose a nonlinear least squares minimization procedure in order to fit the constitutive model proposed in Section 2.2 to the experimental data described in Section 2.1. We set the objective functions to be

$$\mathcal{F}_{uniax}(C,G,a,\varphi)=\sum_{\forall i}\left(\mathbf{P}_{11}(\tilde{\lambda}_c^{(i)})-\tilde{\mathbf{P}}_c^{(i)}\right)^2 \tag{11}$$

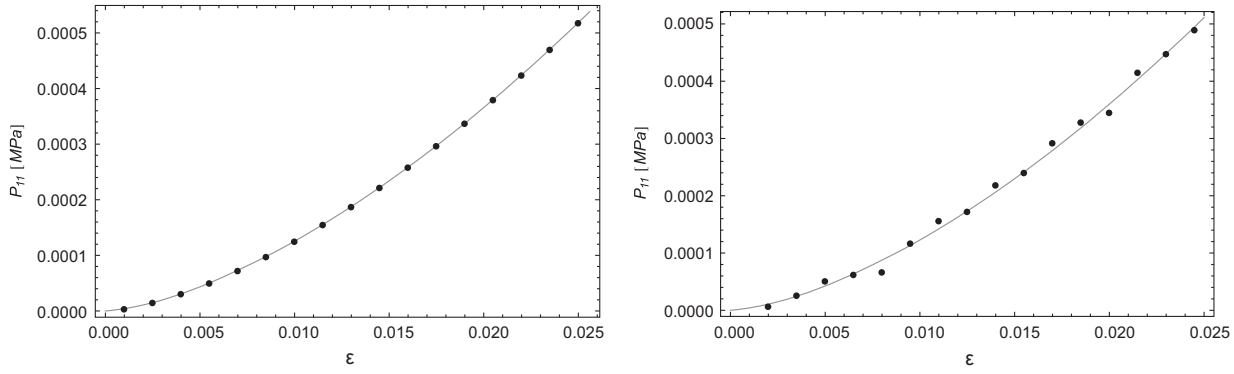

Fig. 3. Fitted model (continuous lines) using synthetic data sets (circles) generated with $(C, G, a, \phi)=(0.15\text{ MPa}, 100\text{ MPa}, 2.6, 15^{\circ})$. Left: No noise, estimated parameters $(C, G, a, \phi)=(0.1563\text{ MPa}, 108.2\text{ MPa}, 2.608, 15.74^{\circ})$. Right: Noisy data (additive Gaussian noise with mean 1 and standard deviation 10^{-5}), estimated parameters $(C, G, a, \phi)=(0.1002\text{ MPa}, 120.5\text{ MPa}, 2.654, 13.50^{\circ})$.

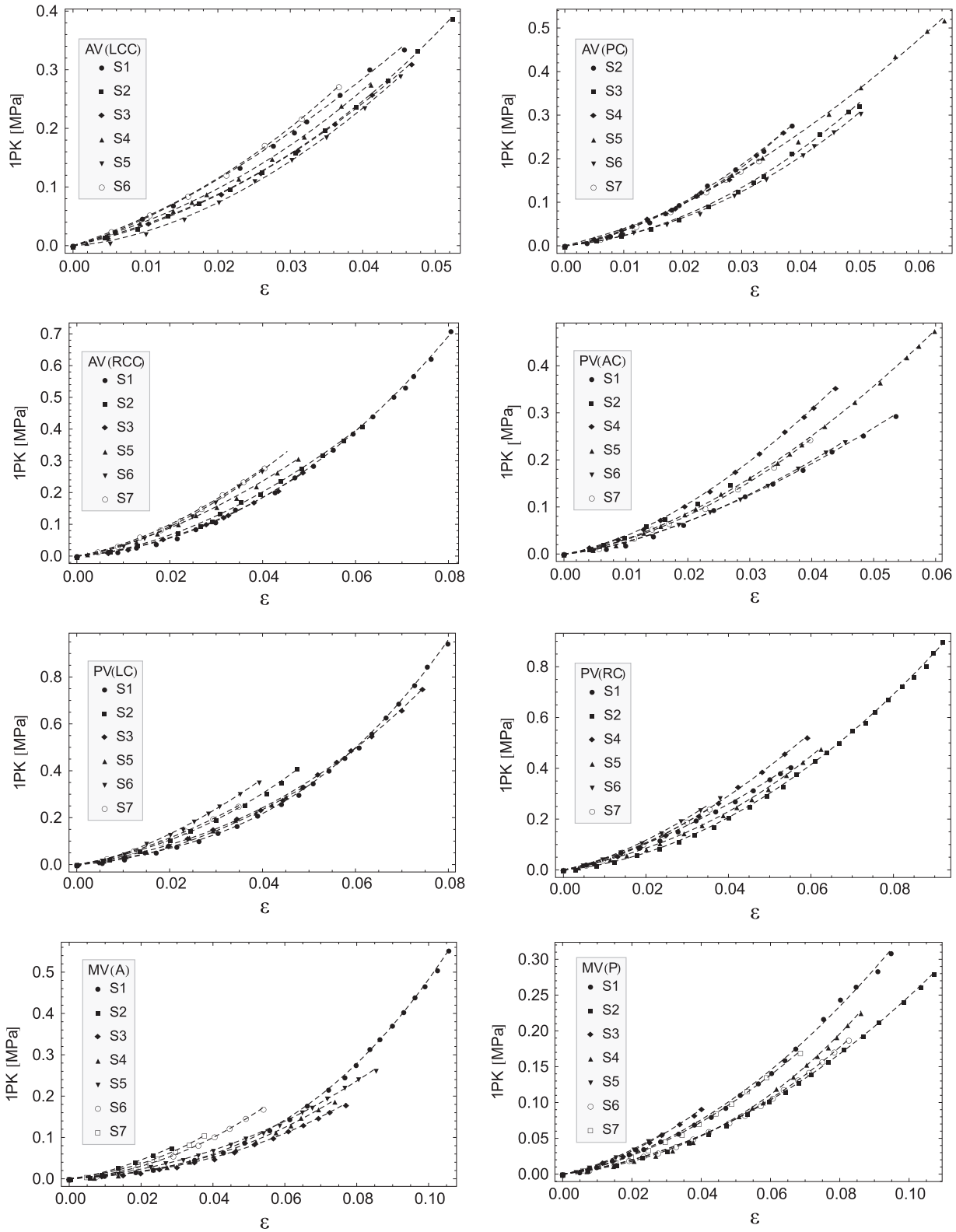

Fig. 4. Uniaxial data set and fitted models for the aortic (LCC, PC, and RCC leaflets), pulmonary (AC, LC, and RC leaflets), and mitral (A and P leaflets) valve. The value ϵ denotes the strain in the direction of applied load following from $\epsilon = \lambda - 1$.

and

$$\mathcal{F}_{biax}(C, G_1, a_1, G_2, a_2, \varphi_1) = \sum_{\forall i} \left(\mathbf{P}_{11}(\tilde{\lambda}_r^{(i)}, \tilde{\lambda}_c^{(i)}) - \tilde{\mathbf{P}}_r^{(i)} \right)^2 + \sum \left(\mathbf{P}_{22}(\tilde{\lambda}_r^{(i)}, \tilde{\lambda}_c^{(i)}) - \tilde{\mathbf{P}}_c^{(i)} \right)^2 \tag{12}$$

for the uniaxial and biaxial data sets, respectively. We furthermore use the relation $\varphi_2 = \varphi_1 + \pi/2$. The tilde in Eqs. (11) and (12) denotes the measured values, and the subscripts r and c denote radial and circumferential directions, respectively. Derivative free numerical minimization of the objective functions was performed in Mathematica using a Nelder–Mead algorithm, whereby each sample was taken into account separately.

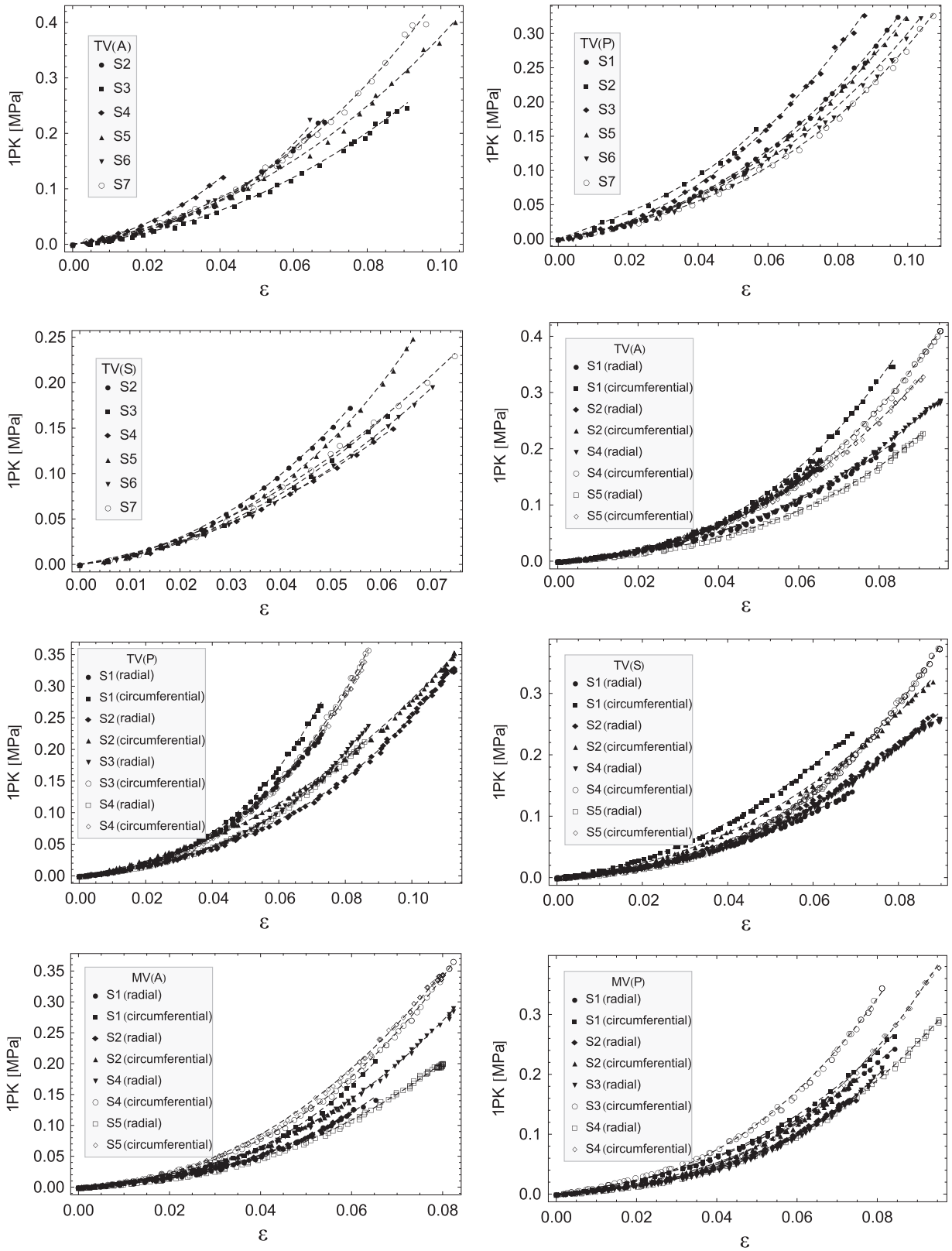

Fig. 5. Uniaxial data set and fitted models for the tricuspid valve (A, P, and S leaflets), and biaxial data set for the tricuspid (A, P, and S leaflets) and mitral (A and P leaflets) valve. The value ϵ denotes the strain in the direction of applied load following from $\epsilon = \lambda - 1$.

2.4. Aortic valve simulation

The goal of this numerical simulation is to show that the estimated parameter values can be straightforwardly used as initial guesses in computational solid mechanics simulations as a proof of concept. For this purpose, we consider a parametric analysis on a patient-specific aortic valve geometry. A surface representation of the aortic valve was first generated from a manual segmentation of a computerized tomography image, and then extruded in order to obtain the final volumetric valve geometry with a uniform wall thickness of 0.6 mm. To verify convergence with respect to mesh size, two tetrahedral computational meshes were generated using `Gmsh` (Geuzaine and Remacle, 2009), with reference mesh

sizes of 0.25 mm and 0.125 mm, respectively (see Fig. 6). For each of the meshes, both linear and quadratic piecewise polynomial ansatz functions for interpolations of the displacement field were tested. The final number of displacement degrees of freedom result in approximately $150 \cdot 10^3$ and $800 \cdot 10^3$ for the linear-, and $950 \cdot 10^3$ and $5.7 \cdot 10^6$ for the quadratic ansatz functions.

The solid mechanics model considered for the aortic valve analysis is based on the classical elastodynamic equations with four physical terms: the inertial forces, viscous Rayleigh damping forces, the internal hyperelastic forces, and the external surface pressure loads. The mass density in the inertia term was taken as 1 gr/cm^3, as usually done for soft tissues. A Rayleigh-type damping matrix, proportional to the tangential stiffness matrix with proportionality constant 10^{-6} s, was included in order to restrict the leaflet oscillation but without overdamping them.

The fiber orientation used in the anisotropic part of the constitutive model was assigned in the circumferential direction as shown in Fig. 6. To reduce computational cost, we furthermore assume the material as nearly incompressible and add the term $K(J+J^{-1}-2)$ to the material's energy density function (Wiechert et al., 2009), instead of representing the incompressibility explicitly and solving for the Lagrangian multiplier in Eq. (3). Using this approach, we obtain volume changes smaller than 1% for the chosen values of K. The hyperelastic constitutive parameters C, G, a, and K are varied in the range of the fitted values in order to demonstrate the applicability of the results for physiologically relevant simulations.

With regard to the Dirichlet boundary conditions, we impose zero displacements on the thin surface in contact with the aortic root, i.e., we model it as belonging to neither the aortic nor the ventricular side. We then proceed as follows for the Neumann boundary conditions: we first obtain ventricular and aortic pressure curves from a lumped parameter model of the heart and aorta, which was calibrated to obtain pressures of 80 and 120 mmHg during diastolic and systolic phases, respectively, see Fig. 7 (left). Then, we apply the pressure load difference between both sides (see Fig. 7 (right)) on the ventricular side only, while no load is applied on the aortic side. This is justified since no prestress is included in the model.

The time marching scheme was chosen as a generalized alpha method with a time step size of 0.25 ms, and the simulations were run up to 40 ms. The computation for the linear displacement fields took 1–3 h on 16 Intel Opteron cores to complete. For the quadratic displacement field, simulations took ~4 h using 48 cores for the coarser mesh and ~24 h using 96 cores for the finer mesh.

Compatibility of analytical expressions and finite element simulations was furthermore validated using uni- and biaxial loading setups (supplementary material).

3. Results

3.1. Measured curves and constitutive parameter fitting

The estimation framework was first assessed using synthetic data, yet disturbed by adding Gaussian noise and undersampling the data set in order to resemble the experimental data. The errors in the estimated parameters with respect to the ground truth were typically around 30% for C, 2% for a, 20% for G and 15% for φ. The larger error for C may be explained due to the fact that for smaller strains, the effect of the elastic matrix dominates and thus the signal-to-noise-ratio is higher than in the large deformation range, in which fiber contributions dominate. Fig. 3 shows a representation of synthetic fittings using undersampled data sets with added noise.

For each different valve and leaflet type, detailed minimization results are given in Figs. 4 and 5 in the form of measured and fitted stress–strain curves. The complete set of estimated parameter values is furthermore tabulated in the appendices. Table 1 summarizes the minimization results for each valve type in terms of the estimated parameter ranges. As can be observed, uniaxial and biaxial tests show systematic differences. The elastic matrix constitutive parameter C ranges between 0.1 and 0.95 MPa in case of

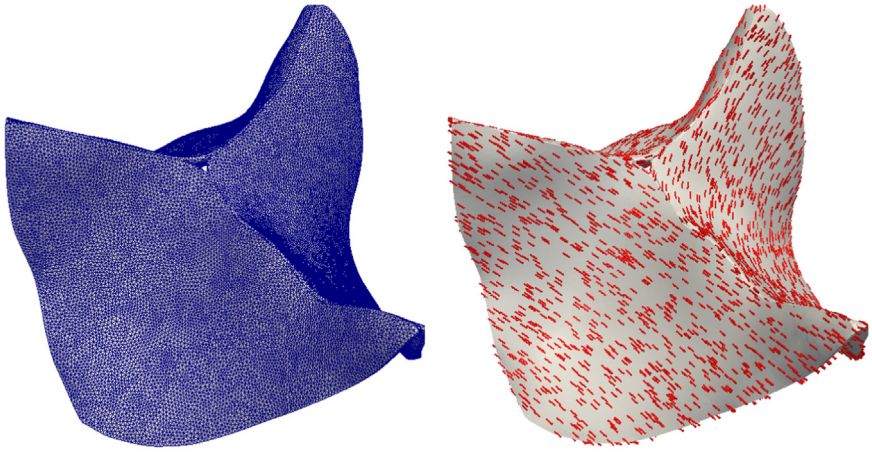

Fig. 6. Computational mesh (mesh size 0.25 mm) of the aortic valve (left) and assigned circumferential fiber family (right). The aortic valve geometry was created from computed tomography data from a 71-year-old male individual with no known valve disease.

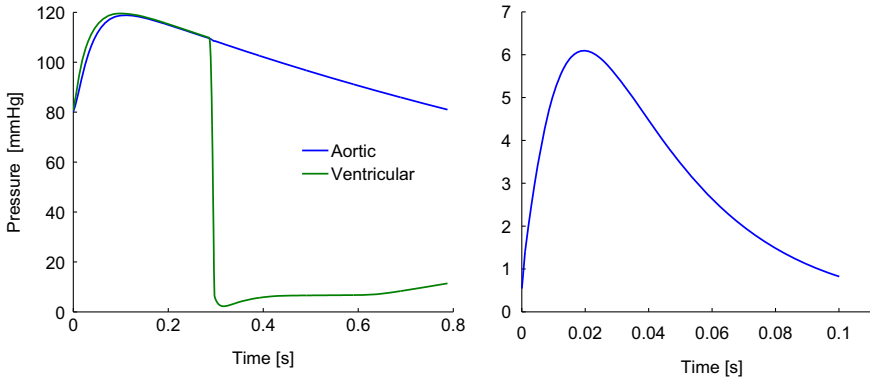

Fig. 7. Ventricular and aortic pressure curves (left) and pressure difference applied at the ventricular side (right).

uniaxial- and between 0.03 and 0.08 MPa in case of biaxial testing. Both fiber stiffness G as well as fiber exponent a on the other hand show systematically larger values in the biaxial test case.

Note that in the tested range of stretches ($(\sqrt{I_{4,i}}-1)<1$), larger exponents a imply a more compliant behavior, whereas larger values of G denote an increase in stiffness. For both biaxial and uniaxial cases, stress–strain curves of the same leaflet types lie within similar ranges, see Figs. 4 and 5 for the mitral and tricuspid valve. For some cases, samples under biaxial loading show a stiffer material behavior, which may be based on differences in the experimental setup (Eilaghi et al., 2009) (clamps are used for the sample-to-actuator connection in uniaxial tests, whereas hooks

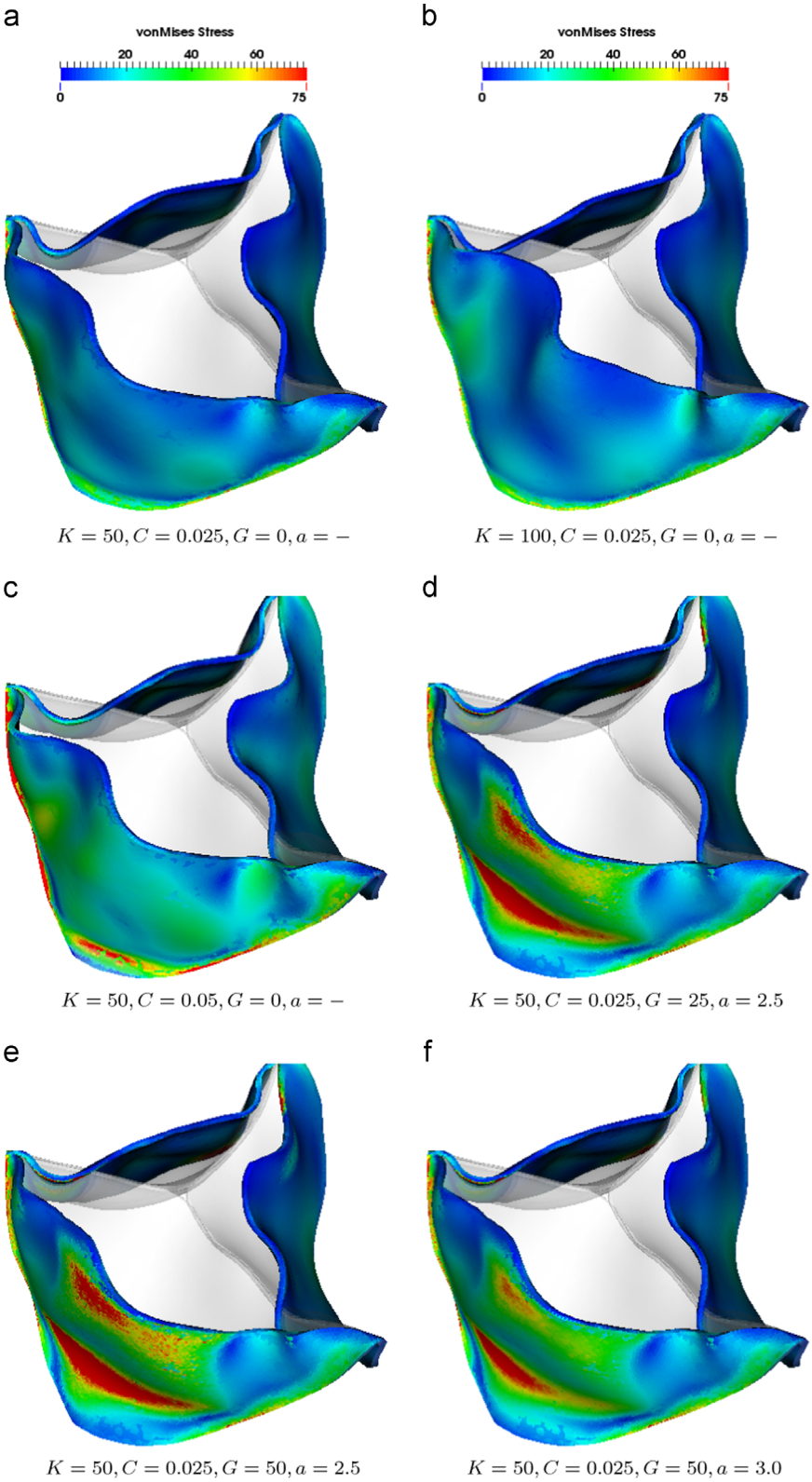

Fig. 8. Von Mises stress at peak systolic pressure difference for different constitutive parameter sets. The gray geometry denotes the reference configuration.

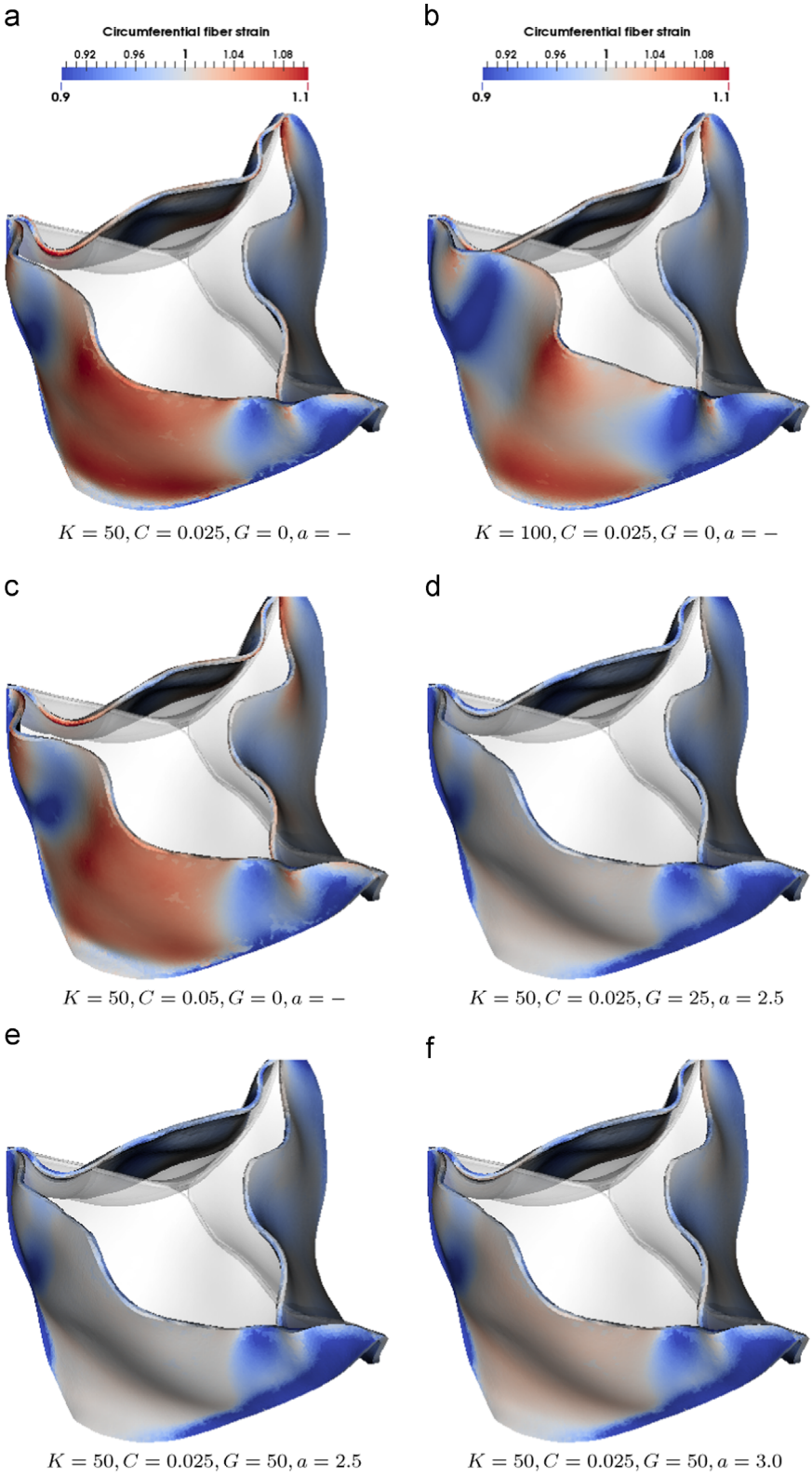

Fig. 9. Circumferential strains at peak systolic pressure difference for different constitutive parameter sets. The gray geometry denotes the reference configuration.

are used in the biaxial cases). Furthermore, sample sizes are increased in the biaxial tests and a larger amount of collagen fibers may be activated during biaxial loading.

Moreover, a comparison of data curves from samples of different ages does not reveal a clear tendency towards a stiffening or softening behavior with increasing age of the leaflet samples in the examined range of zero to three days, which is consistent with similar tests performed on mitral valve tissues of different ages (May-Newman and Yin, 1995). An example of this behavior can be seen in Fig. 4, in which sample *S*1 of the AV (LCC) leaflet was tested at the

day of dissection, whereas samples *S6* and *S2* were tested after one day.

3.2. Aortic valve simulation

The simulation results at peak opening (i.e., 0.04 s) are presented in Figs. 8 and 9 for the coarse quadratic displacement field. Here, we only show the coarse variant, since the relative L_∞-norm respective the displacement fields between the coarse and fine quadratic implementation is smaller than 6%. The relative L_∞-norm of the linear displacement field of the coarse and fine mesh to the fine quadratic values returns values up to 77% and 70%, respectively. These values indicate that the computed linear versions still include a considerable amount of locking effects. Therefore, the rest of the evaluation will be restricted to the quadratic deformation field of the coarse mesh. The computed strain values in the circumferential fiber direction $\sqrt{I_{4,1}}$ are 0.99 $\pm$ 0.05 with fibers and 0.97 $\pm$ 0.03 without fibers (Fig. 9(a) and (f), respectively).

4. Discussion

4.1. Experimental results and parameter fittings

The characterization of the mechanical properties of biological tissues is beset by several well-known difficulties. First, a difficulty that is encountered in reducing the force data to stress data is that the measured thicknesses in all leaflets under consideration are non-uniform. These thickness variations are in particular due to the underlying fiber distributions and orientations and, in the cases of mitral and tricuspid valves, furthermore resulting from papillary muscles which penetrate the tissue at different points, see Fig. 1. It should therefore be carefully noted that in the calculation of stresses from force data, the average thicknesses for every leaflet type are used (see Section 2.1). Naturally, this assumption may lead to additional error sources in the estimation of the constitutive parameters. However, due to the large amount of samples, a semi-analytical fitting procedure was adopted instead of a "sample-specific" inverse analysis. This choice is also supported by the fact that in computational simulations the thickness variations are usually neglected due to the impossibility of segmenting the local tissue structure from standard medical images.

Other experimental artifacts that may potentially influence measurements are the pre-stresses from clamping and the preconditioning procedure. Furthermore, the age of the individuals *prae mortis*, which in the present study varied between six to twelve months, and the state of health of the individuals may also influence the mechanical valve response.

These difficulties and uncertainties notwithstanding, and accounting for the natural variability in properties between individuals, the test data is clearly indicative of a number of fundamental properties of the response of heart valve tissue. These properties include a progressively stiffening response with increasing elongation and a marked anisotropy in tissue elasticity. Some of the material parameters of this work can furthermore be compared to those reported in other contributions. The matrix stiffness C for example, which is the derivative of the strain energy with respect to I_1, can be compared to material constants in the isotropic model case presented in Rausch et al. (2011). For a leaflet thickness of 0.5 mm, the optimal stiffness parameter obtained from inverse finite element analysis using a Neo–Hookean material model thereby lies around 80 MPa, which is well above the upper limit of matrix stiffness of 0.13 MPa for the mitral valve as reported in this work (see Table 1). However, noting that collagenous fibers have been identified as the main load bearing component from our constitutive analysis in the measured range of strains, it is interesting to note that the fiber stiffness G with a maximum value of 102 MPa for the mitral valve as reported here lies within a similar range. Comparably low values of matrix stiffness for fiber-reinforced mitral valve tissue can additionally be found in Prot et al. (2009), in which values as low as 0.001 MPa are reported for the posterior leaflet of a healthy human mitral valve.

4.2. Constitutive model

Prominant models for fiber-reinforced heart valve tissues that have been proposed in the literature are most commonly exponential-type constitutive models of the general form

$$W_{\text{fiber}} = c_0(\exp(c_1 Q^a) - 1)\,,\ Q = |I_{4f}^q - 1|_+\,, \tag{13}$$

with typical combinations $\{q,a\} = \{1,1\}$ (Billiar and Sacks, 2000a; Driessen et al., 2005; Soares et al., 2014), $\{q,a\} = \{1,2\}$ (Prot et al., 2007, 2009) or $\{q,a\} = \{1/2,4\}$ (Chen et al., 2004; May-Newman and Yin, 1998; Prot et al., 2007, 2009). The fiber model proposed in this work matches (13) with $q = 1/2$ to first order, i.e.,

$$W_{\text{fiber}} = c_0(\exp(c_1 Q^a) - 1) = GQ^a + \mathcal{O}(Q^{2a})\,,\ G = c_0 c_1. \tag{14}$$

Thereby, the first order assumption is a good approximation for the fiber stretches obtained in the ex vivo tensile experiments and computed in the simulations ($Q \approx 0.1$). Our fitting results show that the optimal power parameter a lies between 2 and 4 in all cases. This is consistent with the findings presented in Prot et al. (2009), in which it was shown that stress–strain curves fitted for a fixed model (i.e., a equal to 2 or 4) over- or underestimate the stresses depending on the strain values. We hence find an additional motivation for an estimation of the power constant a as shown in this work, which improves the accuracy of the estimation within the given stress–strain range. Moreover, the first order approximation of the exponential model allows to lump parameters c_0 and c_1 into the fiber stiffness constant $G = c_0 c_1$, so that the proposed strain energy density has the same number of parameters as previously reported models.

4.3. Aortic valve simulations

With regard to the simulations of aortic valve opening, it should be noted that the opening response of the valve is sensitive in the range of chosen parameter values. In particular, the inclusion of the circumferential fiber family flattened the leaflet deformation, diminishing the strains (particularly in the fiber direction, as expected) and increasing the stresses. In order to compare results obtained from finite element simulations (using the parameter values which were estimated in this work) to those reported in other contributions, we resort to measurements of circumferential shortening as given in Thubrikar et al. (1980). There, the elastic modulus of canine aortic valve leaflets was measured in vivo and in vitro, with a measured circumferential shortening between 4% and 15%, which is of similar magnitude as in the results presented in Fig. 9 for circumferential strains at peak systolic pressure difference. For the mitral valve, in vivo strain measurements can furthermore be found in Rausch et al. (2011), with reported values in the same range. Concerning the constitutive parameters, the slightly smaller value of C used in the simulations (compared with estimated values) is expected to compensate deviations from the real physiological values in the loading conditions, thickness, prestress, and/or other neglected mechanical behaviors that are not presented accurately enough in the simulation process.

For the sake of simplicity, our simulations do not include any pre-stresses or pre-strains. We expect a consideration of pre-

stresses to cause: (a) the elastic part (Neo–Hooke) to reduce its contribution to the mechanical response since it diminishes its stiffness with increasing stress, and (b) the collagen fibers to increase their contribution to the response since they become stiffer at higher stresses. A deeper study on this issue lies beyond the scope of this paper, but constitutes an important aspect for future research. Finally, it is worth noting that although the usage of a quadratic displacement field increases the computational cost significantly, its application appears to be necessary in order to achieve mesh-independent results. This necessity could be related to the thin-walled, nearly incompressible and high bending motion nature of a cardiac valve cycle.

The composite material model introduced in this work, together with the tabulated material constants obtained by fitting the experimental data set, provide a basis for the formulation and execution of detailed three-dimensional simulations of heart valve operation under physiological conditions. However, as shown in the simulations, tensile experiments may not be fully representative of the in vivo loading state: the leaflet rather behaves like a “beam” and hence has large parts of tissue subjected to compression. Therefore, moving towards high-resolution in vivo measurements of the kinematics and the loading states is, from the authors point of view, the most necessary step in order to provide a more complete understanding and relevant quantification of valve tissue properties. Some efforts in terms of in vivo strain measurements have been performed for instance for the mitral valve in Rausch et al. (2011).

Conflict of interest statement

None declared.

Acknowledgments

MO and SH gratefully acknowledge support from the Institute for Advanced Study (TU München) through the Hans Fischer Fellowship program. The authors would like to thank the Centre for Radiology, Klinikum rechts der Isar, Munich, for image data used in this work.

Appendix A. Supplementary data

Supplementary data associated with this article can be found in the online version at http://dx.doi.org/10.1016/j.jbiomech.2015.10.043.

References

Billiar, K., Sacks, M., 2000a. Biaxial mechanical properties of the native and glutaraldehyde-treated aortic valve cusp: Part II – a structural constitutive model. J. Biomech. Eng. 122, 327–335.
Billiar, K., Sacks, M., 2000b. Biaxial mechanical properties of the natural and glutaraldehyde treated aortic valve cusp: Part I – experimental results. J. Biomech. Eng. 122, 23–30.
Chen, L., Yin, F.P., May-Newman, K., 2004. The structure and mechanical properties of the mitral valve leaflet-strut chordae transition zone. Trans. ASME 126, 244–251.
Christie, G., Barratt-Boyes, B., 1995. Age-dependent changes in the radial stretch of human aortic valve leaflets determined by biaxial stretching. Ann. Thorac. Surg. 60, S156–S159.
Clark, R., 1973. Stress–strain characteristics of fresh and frozen human aortic and mitral leaflets and chordae tendinae – implications for clinical use. J. Thorac. Cardiovasc. Surg. 66, 202–208.
Driessen, N.J., Bouten, C.V., Baaijens, F.P., 2005. A structural constitutive model for collagenous cardiovascular tissues incorporating the angular fiber distribution. J. Biomech. Eng. 127, 494–503.
Eilaghi, A., Flanagan, J.G., Brodland, G.W., Ethier, C.R., 2009. Strain uniformity in biaxial specimens is highly sensitive to attachment details. J. Biomech. Eng. 131, 091003.
Fung, Y., 1993. Biomechanics: Mechanical Properties of Living Tissues. Springer Verlag, New York.
Geuzaine, C., Remacle, J.F., 2009. Gmsh: a 3-d finite element mesh generator with built-in pre- and post-processing facilities. Int. J. Numer. Methods Eng. 79, 1309–1331.
Hvidberg, E., 1960. Investigation into the effect of mechanical pressure on the water content of isolated skin. Acta Pharm. 16, 245–259.
Lo, D., Vesely, I., 1995. Biaxial strain analysis of the porcine aortic valve. Ann. Thorac. Surg. 60, 374–378.
Marsden, J., Hughes, T., 1983. Mathematical Foundations of Elasticity. Prentice-Hall, Englewood Cliffs, N.J..
May-Newman, K., Yin, F., 1995. Biaxial mechanical behavior of excised porcine mitral valve leaflets. Am. J. Physiol. 269, 1319–1327.
May-Newman, K., Yin, F., 1998. A constitutive law for mitral valve tissue. J. Biomech. Eng. 120, 38–47.
Prot, V., Skallerud, B., Holzapfel, G., 2007. Transversely isotropic membrane shells with application to mitral valve mechanics. Constitutive modeling and finite element implementation. Int. J. Numer. Methods Eng. 71, 987–1008.
Prot, V., Skallerud, B., Sommer, G., Holzapfel, G., 2009. On modeling and analysis of healthy and pathological human mitral valves: two case studies. J. Mech. Behav. Biomed. Mater. 3, 167–177.
Rausch, M., Famaey, N., O'Brien Shultz, T., Bothe, W., Craig Miller, D., Kuhl, E., 2013. Mechanics of the mitral valve – a critical review, an in vivo parameter identification, and the effect of prestrain. Biomech. Model. Mechanobiol., 12.
Rausch, M.K., Bothe, W., Kvitting, J.P.E., Göktepe, S., Miller, D.C., Kuhl, E., 2011. In vivo dynamic strains of the ovine anterior mitral valve leaflet. J. Biomech. 44, 1149–1157.
Rausch, M.K., Kuhl, E., 2013. On the effect of prestrain and residual stress in thin biological membranes. J. Mech. Phys. Solids 61, 1955–1969.
Soares, A.L.F., van Geemen, D., van den Bogaerdt, A.J., Oomens, C.W.J., Bouten, C.V.C., Baaijens, F.P.T., 2014. Mechanics of the pulmonary valve in the aortic position. J. Mech. Behav. Biomed. Mater. 29, 557–567.
Stella, J., Sacks, M., 2007a. On the biaxial mechanical properties of the layers of the aortic valve leaflet. J. Biomech. Eng. 129, 757–766.
Stella, J.L., Sacks, M., 2007b. Time-dependent biaxial mechanical behavior of the aortic heart valve leaflet. J. Biomech. 40, 3169–3177.
Thubrikar, M., Piepgrass, W.C., Bosher, L.P., Nolan, S.P., 1980. The elastic modulus of canine aortic valve leaflets in vivo and in vitro. Circ. Res. 47, 792–800.
Wiechert, L., Metzke, R., Wall, W.A., 2009. Modeling the mechanical behavior of lung tissue at the microlevel. J. Eng. Mech. 135, 434–438.